

# Crossed Nonlinear Dynamical Hall Effect in Twisted Bilayers

Cong Chen,<sup>1,2,\*</sup> Dawei Zhai,<sup>1,2,\*</sup> Cong Xiao,<sup>2,3,†</sup> and Wang Yao<sup>1,2,‡</sup>

<sup>1</sup>New Cornerstone Science Laboratory, Department of Physics, University of Hong Kong, Hong Kong, China

<sup>2</sup>HKU-UCAS Joint Institute of Theoretical and Computational Physics at Hong Kong, Hong Kong, China

<sup>3</sup>Institute of Applied Physics and Materials Engineering, University of Macau, Taipa, Macau, China

We propose a novel nonlinear dynamical Hall effect characteristic of layered materials with chiral symmetry, which is driven by the joint action of in-plane and time variation of out-of-plane ac fields  $\mathbf{j}_H \sim \dot{\mathbf{E}}_{\perp} \times \mathbf{E}_{\parallel}$ . A new band geometric quantity – interlayer Berry connection polarizability, which probes a mixed quantum metric characteristic of layer hybridized electrons by twisted interlayer coupling, underlies this effect. When the two orthogonal fields have common frequency, their phase difference controls the on/off, direction and magnitude of the rectified Hall current. We show sizable effects in twisted homobilayer transition metal dichalcogenides and twisted bilayer graphene over broad range of twist angles. Our work opens the door to discovering mixed quantum metric responses unique to van der Waals stacking and concomitant applications under the nonlinear spotlight.

Nonlinear Hall-type response to an in-plane electric field in a two dimensional (2D) system with time reversal symmetry has attracted marked interests [1–4]. Intensive studies have been devoted to uncovering new types of nonlinear Hall transport induced by quantum geometry [4–6] and their applications such as terahertz rectification [7] and magnetic information readout [8]. Restricted by symmetry [1], the known mechanisms of nonlinear Hall response in quasi-2D nonmagnetic materials [2, 3, 9, 10] are all of extrinsic nature, sensitive to fine details of disorders [11, 12], which have limited their utilization for practical applications.

The intrinsic nonlinear Hall effect independent of scattering, on the other hand, has been attracting increasing interest [13–18], and the very recent observations of it in antiferromagnets spotlight the importance of exploring Hall transport induced by quantum metric [19, 20]. However, the intrinsic nonlinear Hall effect in its conventional paradigm [13] can only appear in magnetic materials.

Moreover, having a single driving field only, the conventional nonlinear Hall effect has not unleashed the full potential of nonlinearity for enabling controlled gate in logic operation, where separable inputs (i.e., in orthogonal directions) are desirable. The latter, in the context of Hall effect, calls for control by both out-of-plane and in-plane electric fields. A strategy to introduce quantum geometric response to out-of-plane field in quasi-2D geometry is made possible in van der Waals (vdW) layered structures with twisted stacking [21–27]. Taking homobilayer as an example, electrons have an active layer degree of freedom that is associated with an out-of-plane electric dipole [28–30], whereas interlayer quantum tunneling rotates this pseudospin about in-plane axes that are of topologically nontrivial textures in the twisted landscapes [31–33]. Such layer pseudospin structures can underlie novel quantum geometric properties when coupled with out-of-plane field.

In this work we unveil a new type of nonlinear Hall effect in time-reversal symmetric twisted bilayers, where an intrinsic Hall current emerges under the combined ac

tion of an in-plane electric field  $\mathbf{E}_{\parallel}$  and an out-of-plane ac field  $\mathbf{E}_{\perp}(t)$ :  $\mathbf{j} \sim \dot{\mathbf{E}}_{\perp} \times \mathbf{E}_{\parallel}$  [see Fig. 1(a)]. Having the two driving fields (inputs) and the current response (output) all orthogonal to each other, the effect is dubbed as the *crossed nonlinear dynamical Hall effect*. This is also the first nonlinear Hall contribution of an intrinsic nature in nonmagnetic materials without external magnetic field, determined solely by the band structures, not relying on extrinsic factors such as disorders and relaxation times. Having two driving fields of the same frequency, a *dc* Hall current develops, whose on/off, direction and magnitude can all be controlled by the phase difference of the two fields. The effect has a novel band geometric origin in the momentum space curl of interlayer Berry connection polarizability (BCP), probes a mixed quantum metric arising from the interlayer hybridization of electronic states under the chiral crystal symmetry, and enables a unique phase tunable rectification in chiral vdW layered materials and a transport probe of them. As examples, we show sizable effects in small angle twisted transition metal dichalcogenides (tTMDs) and twisted bilayer graphene (tBG), as well as tBG of large angles where Umklapp interlayer tunneling dominates.

*Geometric origin of the effect.* A bilayer system couples to in-plane and out-of-plane driving electric fields in completely different ways. The in-plane field couples to the 2D crystal momentum, leading to Berry-phase effects in the 2D momentum space [34]. In comparison, the out-of-plane field is coupled to the interlayer dipole moment  $\hat{p}$  in the form of  $-E_{\perp}\hat{p}$ , where  $\hat{p} = ed_0\hat{\sigma}_z$  with  $\hat{\sigma}_z$  as the Pauli matrix in the layer index subspace and  $d_0$  the interlayer distance. When the system has a more than twofold rotational axis in the  $z$  direction, as in tBG and tTMDs, any in-plane current driven by the out-of-plane field alone is forbidden. It also prohibits the off-diagonal components of the symmetric part of the conductivity tensor  $\sigma_{ab} = \partial j_a / \partial E_{\parallel,b}$  with respect to the in-plane input and output. Since the antisymmetric part of  $\sigma_{ab}$  is not allowed by the Onsager reciprocity in nonmagnetic systems, all the off-diagonal components of  $\sigma_{ab}$  are for-

bidden, irrespective of the order of out-of-plane field. On the other hand, as we will show, an in-plane Hall conductivity  $\sigma_{xy} = -\sigma_{yx}$  can still be driven by the product of an in-plane field and the time variation rate of an out-of-plane ac field.

To account for the effect, we make use of the semiclassical theory [13, 34–36]. The velocity of an electron is given by

$$\dot{\mathbf{r}} = \frac{1}{\hbar} \partial_{\mathbf{k}} \tilde{\varepsilon} - \frac{e}{\hbar} \mathbf{E}_{\parallel} \times \boldsymbol{\Omega}_{\mathbf{k}} - \boldsymbol{\Omega}_{\mathbf{k}E_{\perp}} \dot{E}_{\perp}, \quad (1)$$

with  $\hbar\mathbf{k}$  as the 2D crystal momentum. Here and hereafter we suppress the band index for simplicity, unless otherwise noted. For the velocity at the order of interest, the  $k$ -space Berry curvature  $\boldsymbol{\Omega}_{\mathbf{k}}$  is corrected to the first order of the variation rate of out-of-plane field  $\dot{E}_{\perp}$ :

$$\boldsymbol{\Omega}_{\mathbf{k}} = \partial_{\mathbf{k}} \times (\mathcal{A} + \mathcal{A}^{\dot{E}_{\perp}}). \quad (2)$$

Here  $\mathcal{A} = \langle u_{\mathbf{k}} | i \partial_{\mathbf{k}} | u_{\mathbf{k}} \rangle$  is the unperturbed  $k$ -space Berry connection, with  $|u_{\mathbf{k}}\rangle$  being the cell-periodic part of the Bloch wave, whereas

$$\mathcal{A}^{\dot{E}_{\perp}}(\mathbf{k}) = \mathcal{G}(\mathbf{k}) \dot{E}_{\perp} \quad (3)$$

is its gauge invariant correction [34, 37, 38], which can be identified physically as an in-plane positional shift of an electron [13] induced by the time evolution of the out-of-plane field. For a band with index  $n$ , we have (details in the Supplemental Material [39])

$$\mathcal{G}^n(\mathbf{k}) = 2\hbar^2 \text{Re} \sum_{m \neq n} \frac{p^{nm}(\mathbf{k}) v^{mn}(\mathbf{k})}{[\varepsilon_n(\mathbf{k}) - \varepsilon_m(\mathbf{k})]^3}, \quad (4)$$

whose numerator involves the interband matrix elements of the interlayer dipole and velocity operators, and  $\varepsilon_n$  is the unperturbed band energy.

Meanwhile, up to the first order of in-plane field, the hybrid Berry curvature in  $(\mathbf{k}, E_{\perp})$  space reads  $\boldsymbol{\Omega}_{\mathbf{k}E_{\perp}} = \partial_{\mathbf{k}}(\mathfrak{A} + \mathfrak{A}^{E_{\perp}}) - \partial_{E_{\perp}}(\mathcal{A} + \mathcal{A}^{E_{\perp}})$ . Here  $\mathcal{A}^{E_{\perp}}$  is the  $k$ -space Berry connection induced by  $E_{\parallel}$  field [13, 36], which represents an intralayer positional shift and whose detailed expression is not needed for our purpose.  $\mathfrak{A} = \langle u_{\mathbf{k}} | i \partial_{E_{\perp}} | u_{\mathbf{k}} \rangle$  is the  $E_{\perp}$ -space Berry connection [40], and

$$\mathfrak{A}^{E_{\perp}}(\mathbf{k}) = \frac{e}{\hbar} \mathcal{G}(\mathbf{k}) \cdot \mathbf{E}_{\parallel} \quad (5)$$

is its first order correction induced by the in-plane field. In addition,  $\tilde{\varepsilon} = \varepsilon + \delta\varepsilon$ , where  $\delta\varepsilon = e\mathbf{E}_{\parallel} \cdot \mathcal{G}\dot{E}_{\perp}$  is the field-induced electron energy [35].

Given that  $\mathfrak{A}^{E_{\perp}}$  is the  $E_{\perp}$ -space counterpart of intralayer shift  $\mathcal{A}^{E_{\perp}}$ , and that  $E_{\perp}$  is conjugate to the interlayer dipole moment, we can pictorially interpret  $\mathfrak{A}^{E_{\perp}}$  as the interlayer shift induced by in-plane field. It indeed has the desired property of flipping sign under the horizontal mirror-plane reflection, hence is analogous to

the so-called interlayer coordinate shift introduced in the study of layer circular photogalvanic effect [40], which is nothing but the  $E_{\perp}$ -space counterpart of the shift vector well known in the nonlinear optical phenomenon of shift current. Therefore, the  $E_{\perp}$ -space BCP  $e\mathcal{G}/\hbar$  can be understood as the interlayer BCP. This picture is further augmented by the connotation that the interlayer BCP is featured exclusively by interlayer-hybridized electronic states: According to Eq. (S2), if the state  $|u_n\rangle$  is fully polarized in a specific layer around some momentum  $\mathbf{k}$ , then  $\mathcal{G}(\mathbf{k})$  is suppressed.

With the velocity of individual electrons, the charge current density contributed by the electron system can be obtained from  $\mathbf{j} = e \int [d\mathbf{k}] f_0 \dot{\mathbf{r}}$ , where  $[d\mathbf{k}]$  is shorthand for  $\sum_n d^2\mathbf{k}/(2\pi)^2$ , and the distribution function is taken to be the Fermi function  $f_0$  as we focus on the intrinsic response. The band geometric contributions to  $\dot{\mathbf{r}}$  lead to a Hall current

$$\mathbf{j} = \chi^{\text{int}} \dot{E}_{\perp} \times \mathbf{E}_{\parallel}, \quad (6)$$

where

$$\chi^{\text{int}} = \frac{e^2}{\hbar} \int [d\mathbf{k}] f_0 [\partial_{\mathbf{k}} \times \mathcal{G}(\mathbf{k})]_z \quad (7)$$

is intrinsic to the band structure. This band geometric quantity measures the  $k$ -space curl of the interlayer BCP over the occupied states, and hence is also a characteristic of layer-hybridized electronic states. Via an integration by parts, it becomes clear that  $\chi^{\text{int}}$  is a Fermi surface property. Since  $\chi^{\text{int}}$  is a time-reversal even pseudoscalar, it is invariant under rotation, but flips sign under space inversion, mirror reflection and rotoreflection symmetries. As such,  $\chi^{\text{int}}$  is allowed if and only if the system possesses a chiral crystal structure, which is the very case of twisted bilayers [40, 41]. Moreover, since twisted structures with opposite twist angles are mirror images of each other, whereas the mirror reflection flips the sign of  $\chi^{\text{int}}$ , the direction of Hall current can be reversed by reversing twist direction.

*Quantum metric nature of the effect.* Given the recent intensive studies on nonlinear Hall transport induced by  $k$ -space quantum metric [19, 20, 42], it is interesting to point out that our proposed effect is ultimately related to the mixed quantum metric in  $(\mathbf{k}, E_{\perp})$  space, which is unique to 2D layered materials. The interlayer BCP can be cast into  $\mathcal{G}^n = -2\hbar \sum_{m \neq n} \mathbf{g}^{nm} / (\varepsilon_n - \varepsilon_m)$ , where  $\mathbf{g}^{nm} = \text{Re}[\langle \partial_{E_{\perp}} u_n | u_m \rangle \langle u_m | \partial_{\mathbf{k}} u_n \rangle]$  has the meaning of the quantum metric in  $(\mathbf{k}, E_{\perp})$  space for a pair of bands  $n$  and  $m$ , in parallel to the familiar  $k$ -space quantum metric for a pair of bands [42–44] (details in [39]). It is gauge invariant and related to the Fubini-Study metric [45]  $\mathbf{g}^n = \text{Re}[\langle \partial_{E_{\perp}} u_n | (1 - |u_n\rangle \langle u_n|) \partial_{\mathbf{k}} u_n \rangle]$  in  $(\mathbf{k}, E_{\perp})$  space as  $\mathbf{g}^n = \sum_{m \neq n} \mathbf{g}^{nm}$ . Moreover,  $\chi^{\text{int}}$  can be decomposed into the Fubini-Study metric term plus additional

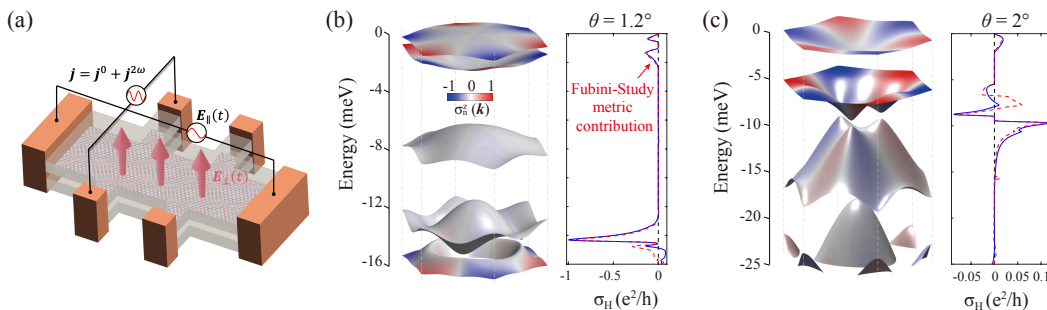


FIG. 1. (a) Schematics of experimental setup. (b, c) Valence band structure and intrinsic Hall conductivity with respect to in-plane input for tMoTe<sub>2</sub> at twist angles (b)  $\theta = 1.2^\circ$  and (c)  $\theta = 2^\circ$  in +K valley. In (b) and (c) the color coding denotes the layer composition  $\sigma_n^z(\mathbf{k})$ , and the red dashed curve denotes the contribution of Fubini-Study metric term.

interband contribution (AIC)

$$\chi^{\text{int}} = 2\hbar e^2 \sum_n \int \frac{d\mathbf{k}}{(2\pi)^2} \frac{\partial f_0}{\partial \varepsilon_n} \frac{(\mathbf{v}^n \times \mathbf{g}^n)_z}{\varepsilon_n - \varepsilon_{\bar{n}}} + \chi_{\text{AIC}}^{\text{int}}, \quad (8)$$

where  $\mathbf{v}^n = \partial \varepsilon_n / \hbar \partial \mathbf{k}$ , and  $\bar{n}$  denotes the band whose energy is closest to  $n$ . In both tTMD and TBG, we find that the Fubini-Study metric term strongly dominates (shown below in Figs. 1(b, c) and Figs. 3(e, f)).

**Phase tunable Hall rectification.** This effect can be utilized for the rectification and frequency doubling of an in-plane ac input  $\mathbf{E}_{\parallel} = \mathbf{E}_{\parallel}^0 \cos \omega t$ , provided that the out-of-plane field has the same frequency, namely  $E_{\perp} = E_{\perp}^0 \cos(\omega t + \varphi)$ . The phase difference  $\varphi$  between the two fields plays an important role in determining the Hall current, which takes the form of

$$\mathbf{j} = \mathbf{j}^0 \sin \varphi + \mathbf{j}^{2\omega} \sin(2\omega t + \varphi). \quad (9)$$

Here  $\omega$  is required to be below the threshold for direct interband transition in order to validate the semiclassical treatment, and

$$\mathbf{j}^0 = \mathbf{j}^{2\omega} = \sigma_{\text{H}} \hat{\mathbf{z}} \times \mathbf{E}_{\parallel}^0, \quad (10)$$

where  $\sigma_{\text{H}} = \frac{1}{2} \omega E_{\perp}^0 \chi^{\text{int}}$  quantifies the Hall response with respect to the in-plane input.

One notes that the rectified output is allowed only if the two crossed driving fields are not in-phase or anti-phase. Its on/off, chirality (right or left), and magnitude are all controlled by the phase difference of the two fields. Such a unique tunability provides not only a prominent experimental hallmark of this effect, but also a controllable route to Hall rectification. In addition, reversing the direction of the out-of-plane field switches that of the Hall current, which also serves as a control knob.

**Application to tTMDs.** We now study the effect quantitatively in tTMDs, using tMoTe<sub>2</sub> as an example [31, 32] (see details of the continuum model in [41]). For illustrative purposes, we take  $\omega/2\pi = 0.1$  THz and  $E_{\perp}^0 d_0 = 10$  mV [21, 26, 27] in what follows.

Figures 1(b) and (c) present the electronic band structures at twist angles  $\theta = 1.2^\circ$  and  $\theta = 2^\circ$ . In both cases,

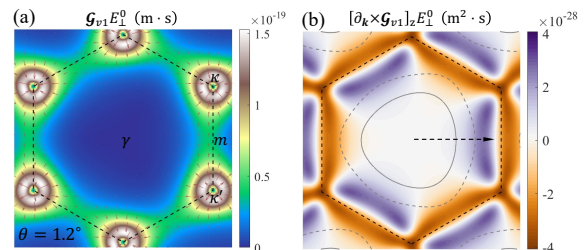


FIG. 2. (a) The interlayer BCP  $\mathcal{G}$ , and (b) its vorticity  $[\partial_{\mathbf{k}} \times \mathcal{G}]_z$  on the first valence band from +K valley of  $1.2^\circ$  tMoTe<sub>2</sub>. Background color and arrows in (a) denote the magnitude and vector flow, respectively. Grey curves in (b) show energy contours at 1/2 and 3/4 of the band width. The black dashed arrow denotes direction of increasing hole doping level. Black dashed hexagons in (a, b) denote the boundary of moiré Brillouin zone (mBZ).

the energy spectra exhibit isolated narrow bands with strong layer hybridization. At  $\theta = 1.2^\circ$ , the conductivity shows two peaks  $\sim 0.1e^2/h$  at low energies associated with the first two valence bands. At higher hole-doping levels, a remarkable conductivity peak  $\sim e^2/h$  appears near the gap separating the fourth and fifth bands. At  $\theta = 2^\circ$ , the conductivity shows smaller values, but the overall trends are similar: A peak  $\sim \mathcal{O}(0.01)e^2/h$  appears at low energies, while larger responses  $\sim \mathcal{O}(0.1)e^2/h$  can be spotted as the Fermi level decreases.

One can understand the behaviors of  $\sigma_{\text{H}}$  from the interlayer BCP in Eq. (S2). It favors band near-degeneracy regions in  $k$ -space made up of strongly layer hybridized electronic states. As such, the conductivity is most pronounced when the Fermi level is located around such regions, which directly accounts for the peaks of response in Fig. 1(b) [and 1(c)]. When the Fermi level is located on the third valence band in Fig. 1(b), the effect is vanishingly small due to the large gaps to adjacent bands.

Let us take the case of Fermi level being located within the first valence band of  $1.2^\circ$  tMoTe<sub>2</sub> in Fig. 1(b) as an example and explain the emergence of the first conductivity peak. The  $k$ -space distributions of  $\mathcal{G}$  and  $[\partial_{\mathbf{k}} \times \mathcal{G}]_z$

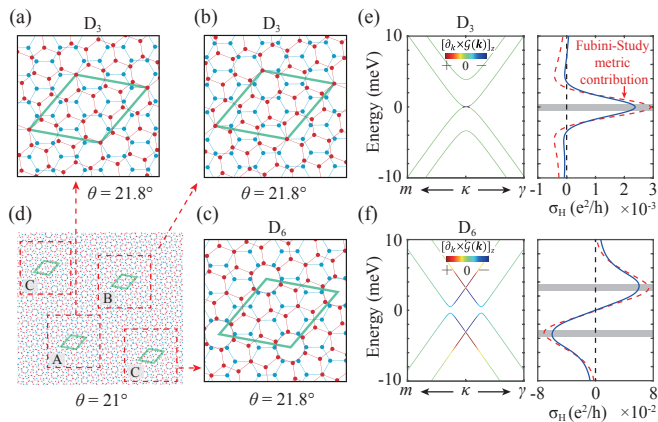


FIG. 3. (a-c) Three high-symmetry stacking registries for tBG with a commensurate twist angle  $\theta = 21.8^\circ$ . Lattice geometries with rotation center on an overlapping atomic site (a, b) and hexagonal center (c). (d) Schematic of the moiré pattern when the twist angle slightly deviates from  $21.8^\circ$ , here  $\theta = 21^\circ$ . Red squares marked by A, B and C are the local regions that resemble commensurate  $21.8^\circ$  patterns in (a), (b) and (c), respectively. (e, f) Low-energy band structures and intrinsic Hall conductivity of the two geometries [(a) and (b) are equivalent]. The red dashed curve denotes the contribution of Fubini-Study metric term. The shaded areas highlight energy windows  $\sim \hbar\omega$  around band degeneracies where interband transitions, not considered here, may quantitatively affect the conductivity measured.

for this band are shown in Figs. 2(a) and 2(b), respectively.  $\mathcal{G}$  is suppressed around the corners of mBZ, for the states are strongly layer polarized there. Interlayer hybridization becomes stronger as  $\mathbf{k}$  moves away from mBZ corners. In this process, the competition between enlarged  $p^{nm}(\mathbf{k})$  and  $k$ -space local gap renders narrow ring-like structures enclosing the mBZ corners, in which  $\mathcal{G}$  is prominent and points radially inward/outward around  $\kappa/\kappa'$ . The distribution of  $\mathcal{G}$  dictates that of  $[\partial_{\mathbf{k}} \times \mathcal{G}]_z$ . One observes that  $[\partial_{\mathbf{k}} \times \mathcal{G}]_z$  is negligible at lower energies, and it is dominated by positive values as the doping increases, thus the conductivity rises initially. As the doping level is higher, regions of  $[\partial_{\mathbf{k}} \times \mathcal{G}]_z < 0$  start to contribute, thus the conductivity decreases after reaching a maximum.

**Application to tBG.** The second example is tBG. We focus on commensurate twist angles in the large angle limit in the main text [46], which possess moiré-lattice assisted strong interlayer tunneling via Umklapp processes [47]. This case is appealing because the Umklapp interlayer tunneling is a manifestation of discrete translational symmetry of moiré superlattice, which is irrelevant at small twist angles and not captured by the continuum model but plays important roles in physical contexts such as higher order topological insulator [48] and moiré excitons [49–51]. The Umklapp tunneling is strongest for the commensurate twist angles of  $\theta = 21.8^\circ$  and  $\theta = 38.2^\circ$ ,

whose corresponding periodic moiré superlattices have the smallest lattice constant ( $\sqrt{7}$  of the monolayer counterpart). Such a small moiré scale implies that the exact crystalline symmetry, which depends sensitively on fine details of rotation center, has critical influence on low-energy response properties.

To capture the Umklapp tunneling, we employ the tight-binding model [46]. Figures 3(a, b) and (c) show two distinct commensurate structures of tBG at  $\theta = 21.8^\circ$  belonging to chiral point groups  $D_3$  and  $D_6$ , respectively. The atomic configurations in Figs. 3(a, b) are equivalent, which are constructed by twisting AA-stacked bilayer graphene around an overlapping atom site, and that in Fig. 3(c) is obtained by rotating around a hexagonal center. Band structures of these two configurations are drastically different within a low-energy window of  $\sim 10$  meV around the  $\kappa$  point [46]. Remarkably, despite large  $\theta$ , we still get  $\sigma_H \sim \mathcal{O}(0.001) e^2/h$  ( $D_3$ ) and  $\sim \mathcal{O}(0.1) e^2/h$  ( $D_6$ ), which are comparable to those at small angles (cf. Fig. S1 in [39]). Such sizable responses can be attributed to the strong interlayer coupling enabled by Umklapp processes [41, 49–51]. The profiles of  $\sigma_H$  can be understood from the distribution of  $[\partial_{\mathbf{k}} \times \mathcal{G}]_z$ .

Figure 3(d) illustrates the atomic structure of tBG with a twist angle slightly deviating from  $\theta = 21.8^\circ$ , forming a supermoiré pattern [39]. In short range, the local stacking geometries resemble the commensurate configurations at  $\theta = 21.8^\circ$ , while the stacking registries at different locales differ by a translation. Similar to the moiré landscapes in the small-angle limit, there also exist high-symmetry locales: Regions A and B enclose the  $D_3$  structure, and region C contains the  $D_6$  configuration. Position-dependent Hall response is therefore expected in such a supermoiré. As the intrinsic Hall signal from the  $D_6$  configuration dominates [see Figs. 3(e) vs (f)], the net response mimics that in Fig. 3(f). As the twist angle deviates more from  $21.8^\circ$ , both the scales of supermoiré and of the  $D_3$  and  $D_6$  local regions become shorter.

**Discussion.** We have uncovered the intrinsic crossed nonlinear dynamical Hall effect characteristic of layer hybridized electrons in twisted bilayers, elucidated its quantum geometric origin, and showed its sizable values in tMD and tBG. Our focus is on the intrinsic effect, which can be evaluated quantitatively for each material and provides a benchmark for experiments. There may also be extrinsic contributions, similar to the side jump and skew scattering in anomalous Hall effect. They typically have distinct scaling behavior with the relaxation time  $\tau$  from the intrinsic effect, hence can be distinguished from the latter in experiments [3, 5, 12, 52]. Moreover, they are suppressed in the clean limit  $\omega\tau \gg 1$  [12]. In high-quality tBG,  $\tau \sim$  ps at room temperature [53]. Much longer  $\tau$  can be obtained at lower temperatures. In fact, a recent theory explaining well the resistivity of tBG predicted  $\tau \sim 10^{-8}$  s at 10 K [54]. As such, high-quality tBG under low temperatures and sub-terahertz input ( $\omega/2\pi = 0.1$

THz) is located in the clean limit, rendering an ideal platform for isolating the intrinsic effect.

This work paves a new route to driving in-plane response by out-of-plane dynamical control of layered vdW structures [55]. The study can be generalized to other observables such as spin current and spin polarization, and the in-plane driving can be statistical forces, like temperature gradient. Such orthogonal controls rely critically on the nonconservation of layer pseudospin degree of freedom, and constitute an emerging research field at the crossing of vdW materials, layertronics, twistrionics and nonlinear electronics.

This work is supported by the National Key R&D Program of China (Grant No. 2020YFA0309600), the Research Grant Council of Hong Kong (AoE/P-701/20, HKU SRFS2122-7S05), the Croucher Foundation, and New Cornerstone Science Foundation. C.X. also acknowledges support by the UM Start-up Grant (SRG2023-00033-IAPME).

---

\* These authors contributed equally to this work.

† [cong Xiao@um.edu.mo](mailto:cong Xiao@um.edu.mo)

‡ [wang Yao@hku.hk](mailto:wang Yao@hku.hk)

- [1] Inti Sodemann and Liang Fu, “Quantum nonlinear hall effect induced by berry curvature dipole in time-reversal invariant materials,” *Phys. Rev. Lett.* **115**, 216806 (2015).
- [2] Qiong Ma, Su-Yang Xu, Huitao Shen, David MacNeill, Valla Fatemi, Tay-Rong Chang, Andrés M. Mier Valdivia, Sanfeng Wu, Zongzheng Du, Chuang-Han Hsu, Shiang Fang, Quinn D. Gibson, Kenji Watanabe, Takashi Taniguchi, Robert J. Cava, Efthimios Kaxiras, Hai-Zhou Lu, Hsin Lin, Liang Fu, Nuh Gedik, and Pablo Jarillo-Herrero, “Observation of the nonlinear hall effect under time-reversal-symmetric conditions,” *Nature* **565**, 337 (2019).
- [3] Kaifei Kang, Tingxin Li, Egon Sohn, Jie Shan, and Kin Fai Mak, “Nonlinear anomalous hall effect in few-layer wte<sub>2</sub>,” *Nat. Mater.* **18**, 324 (2019).
- [4] Z. Z. Du, Hai-Zhou Lu, and X. C. Xie, “Nonlinear hall effects,” *Nat. Rev. Phys.* **3**, 744–752 (2021).
- [5] Shen Lai, Huiying Liu, Zhaowei Zhang, Jianzhou Zhao, Xiaolong Feng, Naizhou Wang, Chaolong Tang, Yuanda Liu, K. S. Novoselov, Shengyuan A. Yang, and Wei-bo Gao, “Third-order nonlinear hall effect induced by the berry-connection polarizability tensor,” *Nat. Nanotechnol.* **16**, 869 (2021).
- [6] Jiadong Zhou, Wenjie Zhang, Yung-Chang Lin, Jin Cao, Yao Zhou, Wei Jiang, Huifang Du, Bijun Tang, Jia Shi, Bingyan Jiang, Xun Cao, Bo Lin, Qundong Fu, Chao Zhu, Wei Guo, Yizhong Huang, Yuan Yao, Stuart S. P. Parkin, Jianhui Zhou, Yanfeng Gao, Yeliang Wang, Yanglong Hou, Yugui Yao, Kazu Suenaga, Xiaosong Wu, and Zheng Liu, “Heterodimensional superlattice with in-plane anomalous hall effect,” *Nature* **609**, 46–51 (2022).
- [7] Yang Zhang and Liang Fu, “Terahertz detection based on nonlinear hall effect without magnetic field,” *Proc. Natl. Acad. Sci. U.S.A.* **118**, e2100736118 (2021).
- [8] Ding-Fu Shao, Shu-Hui Zhang, Gautam Gurung, Wen Yang, and Evgeny Y. Tsymbal, “Nonlinear anomalous hall effect for néel vector detection,” *Phys. Rev. Lett.* **124**, 067203 (2020).
- [9] Pan He, Gavin Kok Wai Koon, Hiroki Isobe, Jun You Tan, Junxiang Hu, Antonio H Castro Neto, Liang Fu, and Hyunsoo Yang, “Graphene moiré superlattices with giant quantum nonlinearity of chiral bloch electrons,” *Nat. Nanotechnol.* **17**, 378–383 (2022).
- [10] Junxi Duan, Yu Jian, Yang Gao, Huimin Peng, Jinrui Zhong, Qi Feng, Jinhai Mao, and Yugui Yao, “Giant second-order nonlinear hall effect in twisted bilayer graphene,” *Phys. Rev. Lett.* **129**, 186801 (2022).
- [11] Naoto Nagaosa, Jairo Sinova, Shigeki Onoda, A. H. MacDonald, and N. P. Ong, “Anomalous hall effect,” *Rev. Mod. Phys.* **82**, 1539–1592 (2010).
- [12] Z. Z. Du, C. M. Wang, Shuai Li, Hai-Zhou Lu, and X. C. Xie, “Disorder-induced nonlinear hall effect with time-reversal symmetry,” *Nat. Commun.* **10**, 3047 (2019).
- [13] Yang Gao, Shengyuan A. Yang, and Qian Niu, “Field induced positional shift of bloch electrons and its dynamical implications,” *Phys. Rev. Lett.* **112**, 166601 (2014).
- [14] Tobias Holder, Daniel Kaplan, and Binghai Yan, “Consequences of time-reversal-symmetry breaking in the light-matter interaction: Berry curvature, quantum metric, and diabatic motion,” *Phys. Rev. Res.* **2**, 033100 (2020).
- [15] Chong Wang, Yang Gao, and Di Xiao, “Intrinsic nonlinear hall effect in antiferromagnetic tetragonal cumnas,” *Phys. Rev. Lett.* **127**, 277201 (2021).
- [16] Huiying Liu, Jianzhou Zhao, Yue-Xin Huang, Weikang Wu, Xian-Lei Sheng, Cong Xiao, and Shengyuan A. Yang, “Intrinsic second-order anomalous hall effect and its application in compensated antiferromagnets,” *Phys. Rev. Lett.* **127**, 277202 (2021).
- [17] Federico Mazzola, Barun Ghosh, Jun Fujii, Gokul Acharya, Debashis Mondal, Giorgio Rossi, Arun Bansil, Daniel Farias, Jin Hu, Amit Agarwal, Antonio Politano, and Ivana Vobornik, “Discovery of a magnetic dirac system with a large intrinsic nonlinear hall effect,” *Nano Letters* **23**, 902–907 (2023).
- [18] Longjun Xiang, Chao Zhang, Luyang Wang, and Jian Wang, “Third-order intrinsic anomalous hall effect with generalized semiclassical theory,” *Phys. Rev. B* **107**, 075411 (2023).
- [19] Anyuan Gao, Yu-Fei Liu, Jian-Xiang Qiu, Barun Ghosh, Thaís V. Trevisan, Yugo Onishi, Chaowei Hu, Tiema Qian, Hung-Ju Tien, Shao-Wen Chen, *et al.*, “Quantum metric nonlinear hall effect in a topological antiferromagnetic heterostructure,” *Science*, eadfl506 (2023).
- [20] Naizhou Wang, Daniel Kaplan, Zhaowei Zhang, Tobias Holder, Ning Cao, Aifeng Wang, Xiaoyuan Zhou, Feifei Zhou, Zhengzhi Jiang, Chusheng Zhang, *et al.*, “Quantum metric-induced nonlinear transport in a topological antiferromagnet,” *Nature*, 1–2 (2023).
- [21] Eva Y. Andrei and Allan H. MacDonald, “Graphene bilayers with a twist,” *Nat. Mater.* **19**, 1265–1275 (2020).
- [22] Leon Balents, Cory R. Dean, Dmitri K. Efetov, and Andrea F. Young, “Superconductivity and strong correlations in moiré flat bands,” *Nat. Phys.* **16**, 725–733 (2020).
- [23] Dante M. Kennes, Martin Claassen, Lede Xian, Antoine Georges, Andrew J. Millis, James Hone, Cory R. Dean, D. N. Basov, Abhay N. Pasupathy, and Angel Rubio, “Moiré heterostructures as a condensed-matter quantum

- simulator,” *Nat. Phys.* **17**, 155–163 (2021).
- [24] Eva Y. Andrei, Dmitri K. Efetov, Pablo Jarillo-Herrero, Allan H. MacDonald, Kin Fai Mak, T. Senthil, Emanuel Tutuc, Ali Yazdani, and Andrea F. Young, “The marvels of moiré materials,” *Nat. Rev. Mater.* **6**, 201–206 (2021).
- [25] Chun Ning Lau, Marc W. Bockrath, Kin Fai Mak, and Fan Zhang, “Reproducibility in the fabrication and physics of moiré materials,” *Nature* **602**, 41–50 (2022).
- [26] Nathan P. Wilson, Wang Yao, Jie Shan, and Xiaodong Xu, “Excitons and emergent quantum phenomena in stacked 2d semiconductors,” *Nature* **599**, 383–392 (2021).
- [27] Emma C. Regan, Danqing Wang, Eunice Y. Paik, Yongxin Zeng, Long Zhang, Jihang Zhu, Allan H. MacDonald, Hui Deng, and Feng Wang, “Emerging exciton physics in transition metal dichalcogenide heterobilayers,” *Nat. Rev. Mater.* **7**, 778–795 (2022).
- [28] P. San-Jose, J. González, and F. Guinea, “Non-abelian gauge potentials in graphene bilayers,” *Phys. Rev. Lett.* **108**, 216802 (2012).
- [29] Dmytro Pesin and Allan H MacDonald, “Spintronics and pseudospintronics in graphene and topological insulators,” *Nat. Mater.* **11**, 409–416 (2012).
- [30] Xiaodong Xu, Wang Yao, Di Xiao, and Tony F Heinz, “Spin and pseudospins in layered transition metal dichalcogenides,” *Nat. Phys.* **10**, 343–350 (2014).
- [31] Fengcheng Wu, Timothy Lovern, Emanuel Tutuc, Ivar Martin, and A. H. MacDonald, “Topological insulators in twisted transition metal dichalcogenide homobilayers,” *Phys. Rev. Lett.* **122**, 086402 (2019).
- [32] Hongyi Yu, Mingxing Chen, and Wang Yao, “Giant magnetic field from moiré induced Berry phase in homobilayer semiconductors,” *Natl. Sci. Rev.* **7**, 12–20 (2020).
- [33] Dawei Zhai and Wang Yao, “Layer pseudospin dynamics and genuine non-abelian berry phase in inhomogeneously strained moiré pattern,” *Phys. Rev. Lett.* **125**, 266404 (2020).
- [34] Di Xiao, Ming-Che Chang, and Qian Niu, “Berry phase effects on electronic properties,” *Rev. Mod. Phys.* **82**, 1959–2007 (2010).
- [35] Cong Xiao, Huiying Liu, Jianzhou Zhao, Shengyuan A. Yang, and Qian Niu, “Thermoelectric generation of orbital magnetization in metals,” *Phys. Rev. B* **103**, 045401 (2021).
- [36] Cong Xiao, Huiying Liu, Weikang Wu, Hui Wang, Qian Niu, and Shengyuan A. Yang, “Intrinsic nonlinear electric spin generation in centrosymmetric magnets,” *Phys. Rev. Lett.* **129**, 086602 (2022).
- [37] D. J. Thouless, “Quantization of particle transport,” *Phys. Rev. B* **27**, 6083–6087 (1983).
- [38] Dimitrie Culcer and Qian Niu, “Geometrical phase effects on the wigner distribution of bloch electrons,” *Phys. Rev. B* **74**, 035209 (2006).
- [39] See Supplemental Material for the detailed derivations of Eqs. (3) – (5) and of the quantum metric related formulas, the effect in tBG with small twist angles, and the elaborated discussion on tBG with twist angle around 21.8°.
- [40] Yang Gao, Yinhan Zhang, and Di Xiao, “Tunable layer circular photogalvanic effect in twisted bilayers,” *Phys. Rev. Lett.* **124**, 077401 (2020).
- [41] Dawei Zhai, Cong Chen, Cong Xiao, and Wang Yao, “Time-reversal even charge hall effect from twisted interface coupling,” *Nature Communications* **14**, 1961 (2023).
- [42] Hikaru Watanabe and Youichi Yanase, “Chiral photocurrent in parity-violating magnet and enhanced response in topological antiferromagnet,” *Phys. Rev. X* **11**, 011001 (2021).
- [43] Junyeong Ahn, Guang-Yu Guo, Naoto Nagaosa, and Ashvin Vishwanath, “Riemannian geometry of resonant optical responses,” *Nature Physics* **18**, 290–295 (2022).
- [44] Pankaj Bhalla, Kamal Das, Dimitrie Culcer, and Amit Agarwal, “Resonant second-harmonic generation as a probe of quantum geometry,” *Phys. Rev. Lett.* **129**, 227401 (2022).
- [45] J. P. Provost and G. Vallee, “Riemannian structure on manifolds of quantum states,” *Commun. Math. Phys.* **76**, 289–301 (1980).
- [46] Pilkyung Moon and Mikito Koshino, “Optical absorption in twisted bilayer graphene,” *Phys. Rev. B* **87**, 205404 (2013).
- [47] E. J. Mele, “Commensuration and interlayer coherence in twisted bilayer graphene,” *Phys. Rev. B* **81**, 161405(R) (2010).
- [48] Moon Jip Park, Youngkuk Kim, Gil Young Cho, and Sung Bin Lee, “Higher-order topological insulator in twisted bilayer graphene,” *Phys. Rev. Lett.* **123**, 216803 (2019).
- [49] Hongyi Yu, Yong Wang, Qingjun Tong, Xiaodong Xu, and Wang Yao, “Anomalous light cones and valley optical selection rules of interlayer excitons in twisted heterobilayers,” *Phys. Rev. Lett.* **115**, 187002 (2015).
- [50] Kyle L Seyler, Pasqual Rivera, Hongyi Yu, Nathan P Wilson, Essance L Ray, David G Mandrus, Jiaqiang Yan, Wang Yao, and Xiaodong Xu, “Signatures of moiré-trapped valley excitons in mose2/wse2 heterobilayers,” *Nature* **567**, 66–70 (2019).
- [51] Long Zhang, Zhe Zhang, Fengcheng Wu, Danqing Wang, Rahul Gogna, Shaocong Hou, Kenji Watanabe, Takashi Taniguchi, Krishnamurthy Kulkarni, Thomas Kuo, Stephen R. Forrest, and Hui Deng, “Twist-angle dependence of moiré excitons in ws2/mose2 heterobilayers,” *Nat. Commun.* **11**, 1–8 (2020).
- [52] Cong Xiao, Hailong Zhou, and Qian Niu, “Scaling parameters in anomalous and nonlinear hall effects depend on temperature,” *Phys. Rev. B* **100**, 161403(R) (2019).
- [53] Luzhao Sun, Zihao Wang, Yuechen Wang, Liang Zhao, Yanglizhi Li, Buhang Chen, Shenghong Huang, Shishu Zhang, Wendong Wang, Ding Pei, Hongwei Fang, Shan Zhong, Haiyang Liu, Jincan Zhang, Lianming Tong, Yulin Chen, Zhenyu Li, Mark H. Rummeli, Kostya S. Novoselov, Hailin Peng, Li Lin, and Zhongfan Liu, “Hetero-site nucleation for growing twisted bilayer graphene with a wide range of twist angles,” *Nat. Commun.* **12**, 2391 (2021).
- [54] Girish Sharma, Indra Yudhistira, Nilotpal Chakraborty, Derek YH Ho, MM Al Ezzi, Michael S Fuhrer, Giovanni Vignale, and Shaffique Adam, “Carrier transport theory for twisted bilayer graphene in the metallic regime,” *Nat. Commun.* **12**, 1–11 (2021).
- [55] Dawei Zhai and Wang Yao, “Ultrafast control of moiré pseudo-electromagnetic field in homobilayer semiconductors,” *Nat. Sci.* **2**, e20210101 (2022).
- [56] Mikito Koshino, Noah F. Q. Yuan, Takashi Koretsune, Masayuki Ochi, Kazuhiko Kuroki, and Liang Fu, “Maximally localized wannier orbitals and the extended hubbard model for twisted bilayer graphene,” *Phys. Rev. X* **8**, 031087 (2018).

- [57] Zhida Song, Zhijun Wang, Wujun Shi, Gang Li, Chen Fang, and B. Andrei Bernevig, “All magic angles in twisted bilayer graphene are topological,” *Phys. Rev. Lett.* **123**, 036401 (2019).

# Supplemental Material

Cong Chen,<sup>1,2,\*</sup> Dawei Zhai,<sup>1,2,\*</sup> Cong Xiao,<sup>2,3,†</sup> and Wang Yao<sup>1,2,‡</sup>

<sup>1</sup>*New Cornerstone Science Laboratory, Department of Physics, University of Hong Kong, Hong Kong, China*

<sup>2</sup>*HKU-UCAS Joint Institute of Theoretical and Computational Physics at Hong Kong, Hong Kong, China*

<sup>3</sup>*Institute of Applied Physics and Materials Engineering, University of Macau, Taipa, Macau, China*

## CONTENTS

References	5
I. Derivation of Eqs. (3) – (5) in the main text	8
II. Quantum metric nature of the effect	9
III. Extra figures for tBG at small twist angles	10
IV. Detailed discussions on tBG with twist angles around 21.8°	12

## I. DERIVATION OF EQS. (3) – (5) IN THE MAIN TEXT

Equation (5) in the main text shows that the first order correction induced by in-plane field to the  $E_{\perp}$ -space Berry connection  $\mathfrak{A} = \langle u_{\mathbf{k}} | i\partial_{E_{\perp}} | u_{\mathbf{k}} \rangle$  is

$$\mathfrak{A}^{E_{\parallel}}(\mathbf{k}) = \frac{e}{\hbar} \mathcal{G}(\mathbf{k}) \cdot \mathbf{E}_{\parallel}. \quad (\text{S1})$$

This can be derived from the field induced correction to the wave function. At the first order of in-plane field, one has [13, 36]

$$|\delta^{E_{\parallel}} u_{n\mathbf{k}}\rangle = \sum_{m \neq n} \frac{-\hbar \mathcal{A}_{mn} \cdot e\mathbf{E}_{\parallel} / \hbar}{\varepsilon_n - \varepsilon_m} |u_{m\mathbf{k}}\rangle,$$

where  $\mathcal{A}_{mn} = \langle u_{m\mathbf{k}} | i\partial_{\mathbf{k}} | u_{n\mathbf{k}} \rangle$  is the  $k$ -space interband Berry connection. We thus have

$$\begin{aligned} \mathfrak{A}^{E_{\parallel}}(\mathbf{k}) &= 2\text{Re} \langle u_{n\mathbf{k}} | i\partial_{E_{\perp}} | \delta^{E_{\parallel}} u_{n\mathbf{k}} \rangle = -2e \sum_{m \neq n} \frac{\text{Re} [\langle u_n | i\partial_{E_{\perp}} | u_m \rangle \langle u_m | i\partial_{\mathbf{k}} | u_n \rangle]}{\varepsilon_n - \varepsilon_m} \cdot \mathbf{E}_{\parallel} \\ &= 2e\hbar \text{Re} \sum_{m \neq n} \frac{p^{nm} \mathbf{v}^{mn}}{(\varepsilon_n - \varepsilon_m)^3} \cdot \mathbf{E}_{\parallel} \\ &= \frac{e}{\hbar} \mathcal{G}(\mathbf{k}) \cdot \mathbf{E}_{\parallel}, \end{aligned}$$

with

$$\mathcal{G}^n = 2\hbar^2 \text{Re} \sum_{m \neq n} \frac{p^{nm} \mathbf{v}^{mn}}{(\varepsilon_n - \varepsilon_m)^3} = -2\hbar \sum_{m \neq n} \frac{\text{Re} [\langle u_n | i\partial_{E_{\perp}} | u_m \rangle \langle u_m | i\partial_{\mathbf{k}} | u_n \rangle]}{\varepsilon_n - \varepsilon_m}, \quad (\text{S2})$$

which proves Eqs. (4) and (5) in the main text.

Equation (3) in the main text shows that the first order correction induced by the time-variation rate of out-of-plane field to the  $k$ -space Berry connection  $\mathcal{A} = \langle u_{\mathbf{k}} | i\partial_{\mathbf{k}} | u_{\mathbf{k}} \rangle$  is

$$\mathcal{A}^{\dot{E}_{\perp}}(\mathbf{k}) = \mathcal{G}(\mathbf{k}) \dot{E}_{\perp} \quad (\text{S3})$$



This can be also derived from the field induced correction to the wave function. At the first order of  $\dot{E}_\perp$ , one has [38]

$$|\delta^{\dot{E}_\perp} u_{n\mathbf{k}}\rangle = \sum_{m \neq n} \frac{-\hbar \mathfrak{A}_{mn} \dot{E}_\perp}{\varepsilon_n - \varepsilon_m} |u_{m\mathbf{k}}\rangle, \quad (\text{S4})$$

where  $\mathfrak{A}_{mn} = \langle u_{m\mathbf{k}} | i\partial_{E_\perp} | u_{n\mathbf{k}} \rangle$  is the  $E_\perp$ -space interband Berry connection. We thus have

$$\mathcal{A}^{\dot{E}_\perp}(\mathbf{k}) = 2\text{Re}\langle u_{n\mathbf{k}} | i\partial_{\mathbf{k}} | \delta^{\dot{E}_\perp} u_{n\mathbf{k}} \rangle = -2\hbar \sum_{m \neq n} \text{Re} \frac{\mathcal{A}_{nm} \mathfrak{A}_{mn}}{\varepsilon_n - \varepsilon_m} \dot{E}_\perp = \mathcal{G}(\mathbf{k}) \dot{E}_\perp,$$

which proves Eq. (3) in the main text.

## II. QUANTUM METRIC NATURE OF THE EFFECT

The very recent experimental observations of intrinsic nonlinear Hall effect in antiferromagnets induced by  $k$ -space quantum metric [19, 20] spotlight the importance of exploring nontrivial response induced by quantum metric in various extended parameter space. Differing from that effect which comes from the  $k$ -space quantum metric and requires time-reversal symmetry breaking, our proposed effect comes from the  $(\mathbf{k}, E_\perp)$ -space quantum metric and can appear in nonmagnetic systems. In this section of the Supplemental Material, we show the quantum metric nature of the intrinsic crossed nonlinear dynamical Hall effect.

The response coefficient of intrinsic crossed nonlinear dynamical Hall effect is

$$\chi^{\text{int}} = \frac{e^2}{\hbar} \int [d\mathbf{k}] f_0 [\partial_{\mathbf{k}} \times \mathcal{G}]_z, \quad (\text{S5})$$

which measures the antisymmetrized  $k$ -space dipole of the interlayer BCP over the occupied states. Via an integration by parts, it becomes

$$\chi^{\text{int}} = -e^2 \int [d\mathbf{k}] f'_0 (\mathbf{v} \times \mathcal{G})_z, \quad (\text{S6})$$

where  $f'_0 = \partial f_0 / \partial \varepsilon_n$ . The numerator of  $\mathcal{G}$  (Eq. (S2))

$$\mathbf{g}^{nm} = \text{Re} [\langle u_n | i\partial_{E_\perp} | u_m \rangle \langle u_m | i\partial_{\mathbf{k}} | u_n \rangle] = \text{Re} [\langle \partial_{E_\perp} u_n | u_m \rangle \langle u_m | \partial_{\mathbf{k}} u_n \rangle] \quad (\text{S7})$$

is the quantum metric in  $(\mathbf{k}, E_\perp)$  space for a pair of bands  $n$  and  $m$ , in parallel to the well-known  $k$ -space quantum metric for a pair of bands  $\tilde{g}_{ij}^{nm} = \text{Re} [\langle \partial_{k_i} u_n | u_m \rangle \langle u_m | \partial_{k_j} u_n \rangle]$  [42-44]. It is gauge invariant and is related to the Fubini-Study quantum metric [45] in  $(\mathbf{k}, E_\perp)$  space as

$$\mathbf{g}^n = \sum_{m \neq n} \mathbf{g}^{nm} = \text{Re} \langle \partial_{E_\perp} u_n | (1 - |u_n\rangle \langle u_n|) | \partial_{\mathbf{k}} u_n \rangle. \quad (\text{S8})$$

The interlayer BCP is thus connected to the mixed quantum metric in  $(\mathbf{k}, E_\perp)$  space:

$$\mathcal{G}^n = -2\hbar \sum_{m \neq n} \frac{\mathbf{g}^{nm}}{\varepsilon_n - \varepsilon_m}. \quad (\text{S9})$$

It can be decomposed into the Fubini-Study metric (FSM) term and an additional interband contribution (AIC)

$$\mathcal{G}^n = \mathcal{G}_{\text{FSM}}^n + \mathcal{G}_{\text{AIC}}^n, \quad (\text{S10})$$

where

$$\mathcal{G}_{\text{FSM}}^n \equiv -2\hbar \frac{\mathbf{g}^n}{\varepsilon_n - \varepsilon_{\bar{n}}}, \quad (\text{S11})$$

$$\mathcal{G}_{\text{AIC}}^n \equiv -2\hbar \sum_{m \neq n, \bar{n}} \mathbf{g}^{nm} \frac{\varepsilon_m - \varepsilon_{\bar{n}}}{(\varepsilon_n - \varepsilon_m)(\varepsilon_n - \varepsilon_{\bar{n}})}, \quad (\text{S12})$$

with  $\bar{n}$  being the band whose energy is closest to  $n$ . Accordingly, the response coefficient of intrinsic crossed nonlinear dynamical Hall effect,

$$\chi^{\text{int}} = 2\hbar e^2 \sum_n \sum_{m \neq n} \int \frac{d\mathbf{k}}{(2\pi)^2} f'_0 \frac{(\mathbf{v}^n \times \mathbf{g}^{nm})_z}{\varepsilon_n - \varepsilon_m}, \quad (\text{S13})$$

is related to the mixed quantum metric in  $(\mathbf{k}, E_\perp)$  space, and can be decomposed into

$$\chi^{\text{int}} = \chi_{\text{FSM}}^{\text{int}} + \chi_{\text{AIC}}^{\text{int}}, \quad (\text{S14})$$

where the U(1) quantum metric term reads

$$\begin{aligned} \chi_{\text{FSM}}^{\text{int}} &\equiv -e^2 \sum_n \int \frac{d\mathbf{k}}{(2\pi)^2} f'_0 (\mathbf{v}^n \times \mathbf{g}_{\text{QM}}^n)_z \\ &= 2\hbar e^2 \sum_n \int \frac{d\mathbf{k}}{(2\pi)^2} f'_0 \frac{(\mathbf{v}^n \times \mathbf{g}^n)_z}{\varepsilon_n - \varepsilon_{\bar{n}}}, \end{aligned} \quad (\text{S15})$$

and the AIC is given by

$$\begin{aligned} \chi_{\text{AIC}}^{\text{int}} &\equiv -e^2 \sum_n \int \frac{d\mathbf{k}}{(2\pi)^2} f'_0 (\mathbf{v}^n \times \mathbf{g}_{\text{AIC}}^n)_z \\ &= 2\hbar e^2 \sum_n \sum_{m \neq n, \bar{n}} \int \frac{d\mathbf{k}}{(2\pi)^2} f'_0 (\mathbf{v}^n \times \mathbf{g}^{nm})_z \frac{\varepsilon_m - \varepsilon_{\bar{n}}}{(\varepsilon_n - \varepsilon_m)(\varepsilon_n - \varepsilon_{\bar{n}})}. \end{aligned} \quad (\text{S16})$$

### III. EXTRA FIGURES FOR TBG AT SMALL TWIST ANGLES

Figure S1(a) shows the band structure of tBG with  $\theta = 1.47^\circ$  obtained from the continuum model [56]. The central bands are well separated from higher ones, and show Dirac points at  $\kappa/\kappa'$  points protected by valley U(1) symmetry and a composite operation of twofold rotation and time reversal  $C_{2z}\mathcal{T}$  [57]. Degeneracies at higher energies can also be identified, for example, around  $\pm 75$  meV at the  $\gamma$  point. As the two Dirac cones from the two layers intersect around the same area, such degeneracies are usually accompanied by strong layer hybridization [see the color in the left panel of Fig. S1(a)]. Additionally, it is well-known that the two layers are strongly coupled when  $\theta$  is around the magic angle ( $\sim 1.08^\circ$ ), rendering narrow bandwidths for the central bands. As discussed in the main text, coexistence of strong interlayer hybridization and small energy separations is expected to contribute sharp conductivity peaks near band degeneracies, as shown in Fig. S1(a). In this case, the conductivity peak near the Dirac point can reach  $\sim 0.1e^2/h$ , while the responses around  $\pm 0.08$  eV are smaller at  $\sim 0.01e^2/h$ .

The above features are maintained when  $\theta$  is enlarged, as illustrated in Figs. S1(b) and (c) using  $\theta = 2.65^\circ$  and  $\theta = 6.01^\circ$ . Since interlayer coupling becomes weaker and the bands are more separated at low energies when  $\theta$  increases, intensity of the conductivity drops significantly.

We stress that  $\mathbf{g}$  is not defined at degenerate points, and interband transitions may occur when energy separation satisfies  $|\varepsilon_n - \varepsilon_m| \sim \hbar\omega$ , the effects of which are not included in the current formulations. Consequently, the results around band degeneracies within energy  $\sim \hbar\omega$  [shaded areas in Fig. S1] should be excluded.

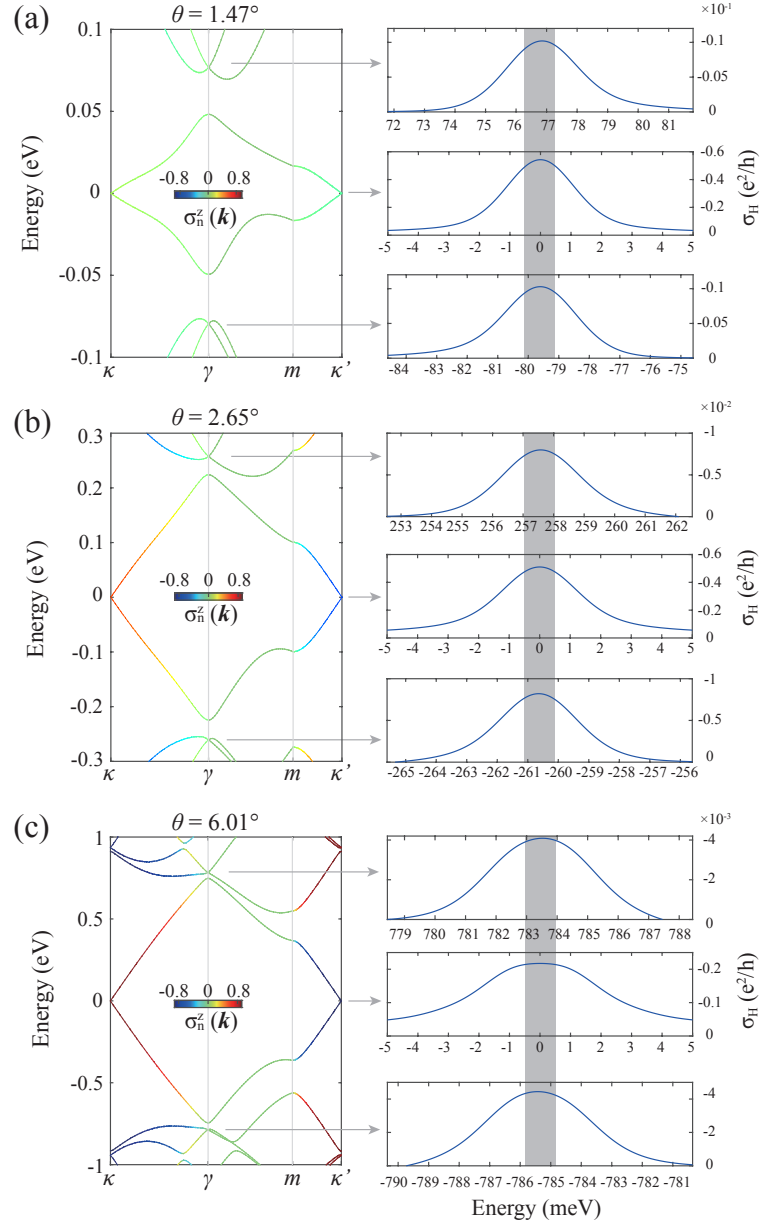


FIG. S1. Band structure and layer composition  $\sigma_n^z$  in +K valley of tBG (left panel) and the intrinsic Hall conductivity (right panel) at three different twist angle  $\theta$ . The shaded areas highlight energy windows  $\sim \hbar\omega$  around band degeneracies in which the conductivity results should not be considered. Here  $\sigma_H$  should be multiplied by a factor of 2 accounting for spin degeneracy.

#### IV. DETAILED DISCUSSIONS ON TBG WITH TWIST ANGLES AROUND $21.8^\circ$

Figure S2(a) shows the two distinct commensurate structures of tBG at  $21.8^\circ$  belonging to chiral point group  $D_3$  and  $D_6$ , respectively. Figures S2(b–d) show lattice structures with various derivations (from large to small) from the commensurate angle  $21.8^\circ$ . Recall that in small-angle moiré patterns, there exist high-symmetry local stacking regions that resemble the commensurate AA, AB, or BA configurations. Likewise, in the supermoiré pattern formed by deviating slightly from  $21.8^\circ$ , there exist local regions enclosed by the circles in Figs. S2(b–d) whose landscapes resemble the commensurate  $D_6$  and  $D_3$  structures in (a). The period of the supermoiré scales linearly with the distance between two adjacent circles. Along the directions of the arrows in Figs. S2(b–d), the local lattice structure smoothly alternates between  $D_3$  and  $D_6$  stackings. When the deviation from  $21.8^\circ$  is small, e.g., Figs. S2(c, d), the supermoiré contains many  $D_3$  and  $D_6$  unit cells. We expect that the Hall conductivity is dominantly contributed by the  $D_6$  stackings. As the derivation gets larger, both the scales of supermoiré and of local regions with commensurate structures become shorter.

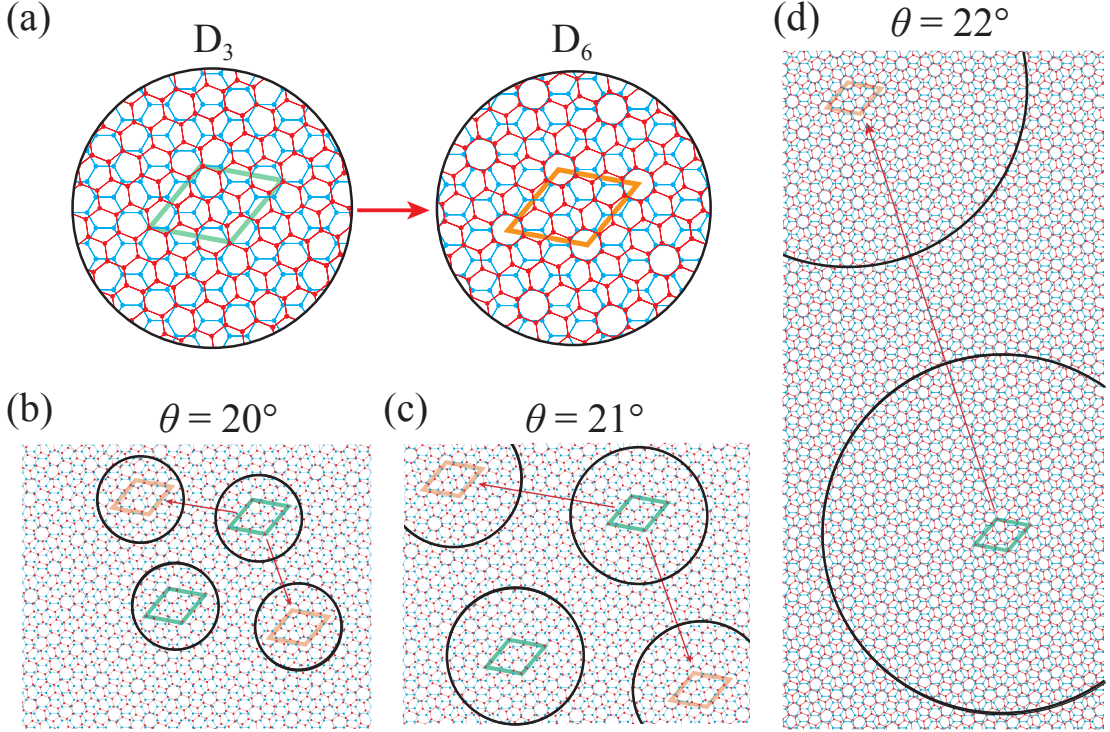


FIG. S2. (a) Commensurate tBG structures at  $\theta = 21.8^\circ$  with  $D_3$  or  $D_6$  symmetries. (b–d) Schematics of supermoiré pattern when twist angle deviates from  $\theta = 21.8^\circ$ . Local regions that resemble the  $D_3$  and the  $D_6$  commensurate structures are enclosed by circles.